Instability and breakup
of a capillary bridge with throughflow:
the "Capillary Venturi"

Gounséti Paré and Jérôme Hoepffner†

UPMC Univ Paris 06 & CNRS, UMR 7190, Institut Jean Le Rond d′Alembert, F-75005 Paris,
France.

The capillary bridge is an axisymmetric body of liquid held between two discs. It has
a rich bifurcations structure, as it can breakup for two different reasons: if its length
is larger than its perimeter, it is unstable to the Rayleigh-Plateau instability, and if its
volume is decreased for a given length and radius, there is a fold bifurcation that leads
to the disappearance of the steady solution. To this classical system we add a dynamic
effect: we consider the behavior of the bridge when there is a flow through it. By analogy
with the instability of a band-saw, we show that the Rayleigh-Plateau instability is a
particular case of the dynamic instability of the capillary Venturi. We compare these
analyses to the nonlinear bifurcation diagram of a 1D model and numerical simulations
of the Navier-Stokes equations.

1. Introduction

The original motivation of this study was atomization: *how a body of fluid can be
transformed into a cloud of droplets*. In Hoepffner & Paré (2013), we studied the retraction
of the tip of a liquid ligament. Because of surface tension, the tip is not a steady state and
it will retract at the Taylor-Culick velocity (see Keller (1983)). As shown in Stone & Leal
(1989) the fluid of the ligament is gathered into a retracting bulb, and a neck appears
between the remaining part of the ligament and the bulb. The presence of this neck
implies that the fluid must accelerate and decelerate before reaching the bulb. The neck
in this retraction behaves like a Venturi flow (Guyon *et al.* (2001)): the flow is accelerated
through the neck (high speed-low pressure) and then decelerated (low speed again, high
pressure again). We have observed that this *capillary Venturi* flow can have interesting
features like nonlinear oscillations and inner jet detachment. The present article is a
dedicated study of the capillary Venturi flow in the simpler configuration sketched in
figure 1.

The historical experiments on the static capillary bridge are described in Plateau
(1873). Because of surface tension, a cylinder of liquid held between two discs will desta-
bilize when its length is larger than its perimeter. It is indeed the necessary condition for
a small perturbation to decrease the total surface. The analysis giving the exponential
growth rate of the different wavelengths on an infinite liquid cylinder is done in Rayleigh
(1879). It is shown that the most rapidly growing wavelength is about $\sqrt{2}$ times the
perimeter. Eggers & Dupont (1994) derive a 1D nonlinear model for this system that
gives more readily the dispersion relation.

The flow that we study here is similar to flows through an elastic pipe, often referred
to as *collapsible tubes*, with applications to blood flows, and originating historically from

† Email address for correspondence: jerome.hoepffner@upmc.fr

2   *G. Paré and J. Hoepffner*
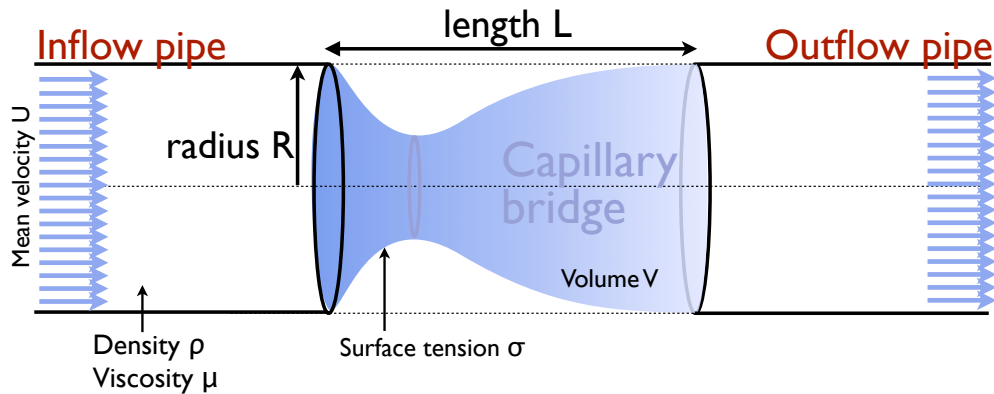
FIGURE 1. Sketch of the flow configuration: a capillary bridge held between two pipes with a throughflow.

the studies of the "Starling resistor"; see for instance Heil & Jensen (2003); Heil & Hazel (2011). In the case of an elastic pipe, in addition to the tension of the membrane, there is bending stiffness and no-slip. This flow can lead to nonlinear self-sustained oscillations, and can also lead to collapse: the low pressure at the neck of the flexible pipe can increase the constriction and so on until blockage.

Capillary bridges with outer axial flow were studied in the context of the float-zone process to produce mono-crystals. One of the limitation for the size of this process is the breakup of large capillary bridges because of gravity. In Russo & Steen (1989); Atreya & Steen (2002), a second liquid is flown upward outside of the capillary bridge to reduce the bulging of the lower part due to gravity. The upward outer flow induces a recirculating zone inside the capillary bridge due to viscous entrainment. This situation with two coaxial fluids is similar to *core-annular* flows, see Joseph *et al.* (1997), used for instance to reduce the pressure drop in flowing viscous fluids through pipes by adding an outer layer of lubricating fluid.

The rivulet of a thin liquid stream flowing on an incline involves instabilities due to the interaction of a throughflow and capillarity, see Grand-Piteira *et al.* (2006); Daerr *et al.* (2011). In this configuration, the flow is not confined by inflow and outflow pipes but is constrained by the motion of contact lines with the incline. The instability is sinuous with wavelength long compared to the width of the rivulet, leading to meanders. In Kirstetter *et al.* (2012), a rivulet interacts with a soap film.

Rosendahl *et al.* (2004); Conrath *et al.* (2013) present experimental studies where a flow interacts with the free surface that contains it. The study is performed in a microgravity environment. Water is flown in a flat channel between two plates and two free surfaces. They demonstrate a critical flow rate for breakup of the free surface. They write that "in current experiments aboard the International Space Station, partially open channels are being investigated to determine critical flow rate-limiting conditions above which the free surface collapses ingesting bubbles." They state that "for such flows, an abrupt transition occurs between steady-state and unsteady *choked* flow conditions, leading to large surface deformations and periodic gas ingestion".

Capillary bridges are also relevant when flowing two immiscible fluids through a porous medium. Because of the flow, the bridges inside of the 3D network are capillary Venturis, see for instance Avraam & Payatakes (1995). In Datta *et al.* (2014), a link is drawn between the breakup of these Venturis due to dynamic effects and the global resistance

to the flow: how much pressure difference do we need to impose between inflow and outflow for a given flux through the porous network. They write in their introduction that "the measured pressure differences are thus interpreted as the pressures dropped in the different fluids, and the relative permeabilities are then calculated using Darcy's law. However, how exactly the two fluids are configured, and how this in turn influences their permeabilities, is poorly understood; indeed, even the validity of the assumption that the fluids flow through connected pathways remain intensely debated (see Richards (1931)). Experiments on a 2D porous medium challenge this notion: in some cases, the non-wetting fluid instead breaks up into discrete ganglia, often as small as the pore size, which are then advected through the medium by the flowing wetting fluid." To explain the transition towards breakup of the capillary Venturis in their 3D experiment, they propose that "the non-wetting fluid breaks up when the sum of the viscous forces exerted by the wetting and the non-wetting fluid exceed the capillary forces at the pore scale."

We remind the behaviour of the static capillary bridge in figure 2, see for instance Lowry & Steen (1995) and Slobozhanin & Perales (1993) or Everett & Haynes (1972). Two parameters are considered: the aspect ratio of the bridge L/R and the volume of the bridge compared to the volume of the cylinder V/V_0. The aspect ratio first matters because of the Rayleigh-Plateau instability. The second parameter is the volume ratio V/V_0: how much thicker or thinner is our bridge compared to a cylinder. We have $V_0 = \pi R^2 L$ and the bridge is a cylinder whenever $V/V_0 = 1$. On the left of the figure (for small L/R) we have two kinds of asymmetric instabilities depending on wether the bridge is thicker or thinner than a cylinder. These two instabilities do not lead to breakup. On the right of the figure we have a boundary beyond which there is no stable bridge, we denote this the "breakup boundary". The bridge may breakup for two different reasons: either when it is *too long*; this phenomenon is related to the Rayleigh-Plateau instability for bridges thicker or thinner than a cylinder, or when it is *too thin*, a case where the steady solution disappear through a fold bifurcation. In this paper we are interested in the way the breakup boundary will change when there is a flow through the bridge.

The goal of the present paper is to present the capillary Venturi as an archetypal configuration to understand how a flow can affect the free surface in which it is contained. To explain the behaviour of this flow we consider theoretically a cylindrical bridge with throughflow. Using an analogy with the instability of a band saw, we give a simple criterion for instability, this is done in §2. This theoretical prediction is then validated against two levels of modeling of the flow: first we compute the bifurcation diagram of a 1D nonlinear model from Eggers & Dupont (1994) in §3, then we perform numerical simulations of the axisymmetric Navier-Stokes equations in §4. We show that these three different points of view coincide qualitatively and quantitatively to provide a rich view of the system.

2. Predicting the breakup of the capillary Venturi

We would like to obtain a criterion for stability or instability of a cylindrical bridge with a given throughflow U. The classical modeling for this would be the *normal-mode* approach, developed originally by Thomson (1871) for the instability of the shear layer and later by Rayleigh (1879) for the instability of the liquid jet. This approach consists in neglecting the longitudinal variations of the base flow and perturbing this spatially-invariant flow system with low amplitude periodic waves. This approach yields the *dispersion relation* of the system: for each wave of a given wavelength λ, the dispersion relation gives the phase speed and the exponential growth rate of the wave. If the growth

4   *G. Paré and J. Hoepffner*

FIGURE 2. Stability of the static capillary bridge. Figure adapted from Lowry & Steen (1995).

rate is positive the wave is unstable, if it is negative, the wave is stable, and if it is zero, the wave is neutral.

In this approach, we assume that the system is infinite and spatially invariant. To recover our flow configuration, we need to account for the presence of boundaries. The constraints imposed by the upstream ($x = 0$) and downstream ($x = L$) boundaries are the following: the free surface deformation should be zero, and the flow velocity should be equal to U. To account for these additional constraints, we build a *global mode* by combining several waves (*normal modes*) of the infinite approximation of the system. Here, there are four constraints (two upstream and two downstream), so we need to combine four waves to be able to satisfy the boundary conditions. This combination of normal modes corresponds to the mutual reflection of the waves against the boundaries: at the right boundary for instance, the waves moving to the right reflects into waves moving to the left. The properties of this reflection are such that the boundary conditions are satisfied. For examples of the method used to build a global mode that satisfies the boundary conditions, please see Doaré & de Langre (2002) or Gallaire *et al.* (2006).

There are many systems where imposing boundary conditions can destabilize a system which would be stable otherwise. Indeed, the boundary conditions can input energy to the system. This implies that depending on the boundary conditions, it is possible to build an unstable global mode by combining neutral or even stable individual waves. This is indeed the case for the two systems that we will consider below: the band-saw, and the capillary Venturi.

In the present section, we present a simpler way to judge for the stability of the bridge. For this we consider that the deformation of the base flow system is the competition

FIGURE 3. Sketch for the Band-saw instability and the analogy with the dynamic instability of the capillary bridge.

of stabilizing and destabilizing forces. For the band-saw, the stability results from the competition of the tension in the saw and the centrifugal force on a curved saw in motion. The system is unstable when the tension is less than the centrifugal destabilizing force. For the capillary bridge, we consider the balance at the free surface between the Laplace pressure jump through the free surface, due to surface tension and curvature, and the hydrodynamic pressure due to the acceleration and deceleration of the flow through the deformed bridge.

For the classical normal mode method, we can choose between a *temporal* or a *spatial* analysis, see for instance Huerre & Monkevitz (1990). In the temporal approach, we impose the wavelength and calculate the associated wavespeed and temporal growth rate. The wave grows in time (unstable) if this growth rate is positive. In the spatial approach on the other hand, we impose the local frequency and calculate the associated wavelength and spatial exponential growth. The waves grow in space if this growth rate is positive. In the present section in contrast, we choose to impose both the wavelength and the wavespeed, and we probe the *force balance*. Thus, the stability/instability limit is found by evaluating an inequality: when the destabilizing forces are larger than the stabilizing forces, the wave is unstable. Imposing the wavelength and the wavespeed is very convenient here because then all boundary conditions are satisfied by default. Indeed, for a stationary wave in the reference frame of the bridge (wavespeed equal to throughflow), satisfying the zero deformation of the interface at $x = 0$ and $x = L$ amounts to selecting wavelengths equal to $2L, L, L/2, L/3, \ldots$.

A first shortcoming of this approach, as compared to the global mode calculation, is that is does not provide the growth rate of the instability. Indeed, forces are not enough to determine the growth rate, we would need to consider as well how masses are moved by these forces. The second shortcoming is that it assumes the destabilization of a static wave, known as *exchange of stability*, which corresponds to a pitchfork bifurcation. We would not be able to capture a Hopf bifurcation for instance. Anyway, we will see that the breakup of the capillary Venturi corresponds indeed to a pitchfork.

2.1. *The example of the band-saw instability*

We start with the straightforward calculation of the band-saw. This classical system is described for instance in Mote (1965); Ulsoy *et al.* (1978). A string under tension is set in motion and glides through two rings, apart by a distance L.

Let us evaluate the force balance on the band. We assume a perturbation to the straight

6   *G. Paré and J. Hoepffner*

configuration in the shape of an arc of circle. Two forces are in competition: the tension of the band on one hand and the centrifugal force on material points traveling along the arc of circle as show on figure 3a). The radius of curvature is R and the velocity is U. The speed of rotation of material points around the geometrical center of the arc of circle is Ω and their velocity is $U = \Omega R$. The centrifugal force per unit length is equal to minus the mass density times the normal acceleration $f = \lambda \Omega^2 R$. We consider the force balance projected in the vertical direction. This yields that the tension applied to the band cannot counteract the centrifugal force whenever

$$Lf > 2T \sin\theta,$$

which yields the critical velocity

$$U > \sqrt{\frac{T}{\lambda}}.$$

The reader has certainly recognized here the wavespeed of the vibrating string. Indeed this instability corresponds to a *supersonic transition*: the saw becomes unstable when its velocity exceeds the speed of its waves. Here we have assumed an initial perturbation in the shape of an arc of circle; the result is identical for a sinusoidal perturbation, after a longer calculation.

2.2. *Pressure balance model for the cylindrical bridge*

We now apply this method to a cylindrical bridge with throughflow. We consider a static deformation of the free surface as sketched in figure 3b), with a throughflow U. We will evaluate the pressure balance between the capillary jump across the curved interface and the hydrodynamic pressure due to the deceleration and acceleration of the fluid through the bulge and the neck as shown on the figure.

The radius of the bridge varies like $r(x)$ with $r(x = 0) = R$. Conservation of flux yields

$$u(x) = \frac{R^2}{r(x)^2} U.$$

We call $p(x = 0) = P_0$ the pressure at inflow. We use the Bernoulli equation to quantify how the variation of velocity affects the hydrodynamic pressure. We assume that the wave is long enough to approximate the velocity at a given section with a plug profile $u(x)$ with $u(x = 0) = U$:

$$\frac{\rho U^2}{2} + P_0 = \frac{\rho u(x)^2}{2} + p(x).$$

Now assuming a small perturbation of the radius $r(x) = R(1 + \varepsilon\delta(x))$ and keeping order one terms in ε (linearizing) we get the expression for the hydrodynamic pressure

$$p(x)_{hydro} = 2\rho U^2 \varepsilon \delta(x) + P_0.$$

We now consider the capillary pressure due to the pressure jump through the interface. This jump is the surface tension σ times the total curvature of the interface. It is positive when the centre of curvature is inside the liquid and negative otherwise. For an axisymmetric interface, the expression is

$$p(x)_{cap} = \sigma \left[\frac{1}{r(1 + r_x^2)^{1/2}} - \frac{r_{xx}}{(1 + r_x^2)^{3/2}} \right],$$

which, after linearization, becomes

$$p(x)_{cap} = \sigma \left(\frac{1 - \varepsilon\delta}{R} - R\varepsilon\delta_{xx} \right).$$

We now consider the balance of pressure at A where the ligaments bulges. We assume a simple shape of the interface perturbation

$$\delta(x) = \cos(\alpha x),$$

with wavenumber α and thus wavelength $2\pi/\alpha$. At A we have $\delta(x = x_A) = 1$ and $\delta_{xx}(x = x_A) = -\alpha^2$.

We can now state the inequality of pressures. The bulge deformation to the cylindrical free surface will increase if the inner hydrodynamic pressure is larger than the capillary pressure (outward acceleration for an outward deformation)

$$p_{hydroA} > p_{capA},$$

that is

$$2\rho U^2 \varepsilon \delta + P_0 > \sigma \left(\frac{1 - \varepsilon\delta}{R} - R\varepsilon\delta_{xx} \right).$$

The reference pressure P_0 is taken at inflow where the axial curvature of the interface is zero thus $P_0 = \sigma/R$; we thus get as a criterion for instability

$$\frac{2\rho U^2}{\sigma} > \frac{-1}{R} + \alpha^2 R$$

which we rewrite more conveniently

$$\frac{U}{U_{cap}} > \sqrt{\frac{(2\pi R/\lambda)^2 - 1}{2}} \tag{2.1}$$

where $U_{cap} = \sqrt{\sigma/(\rho R)}$ is a capillary velocity built from dimensional analysis, and $\lambda = 2\pi/\alpha$ is the wavelength. Consideration of the pressure balance at B gives the same inequality: at B, the free surface has a trough, and when the inequality is satisfied this trough is amplified because the capillary pressure is larger than the hydrodynamic pressure.

For parameters where the inequality becomes an equality, the forces are in balance and the deformation is neutral. These parameters corresponds to waves propagating at wavespeed c without change in amplitude

$$c = U_{cap} \sqrt{\frac{(2\pi R/\lambda)^2 - 1}{2}}. \tag{2.2}$$

We will validate this result in the next section when deriving the dispersion relation of the 1D model from Eggers & Dupont (1994). When the wavelength is longer than the perimeter $2\pi R$ of the cylinder, the argument of the square root of (2.2) becomes negative. This transition corresponds to the classical Rayleigh-Plateau instability, which is safely recovered with the present approach. Waves shorter than the perimeter of the cylinder $\lambda < 2\pi R$ on the other hand are neutral. Our inequality shows that the breakup of the capillary bridge with throughflow, just like for the band-saw, corresponds to a supersonic transition.

As compared to the classical Rayleigh-Plateau instability, we have added in our analysis a throughflow. Because of galilean invariance, this throughflow plays a role thanks to the boundary conditions. When this throughflow vanishes we recover the classical results and we see that adding the throughflow increases the range of unstable waves. Thus we can say that the Rayleigh-Plateau instability is a special case of the instability of the

8   G. Paré and J. Hoepffner
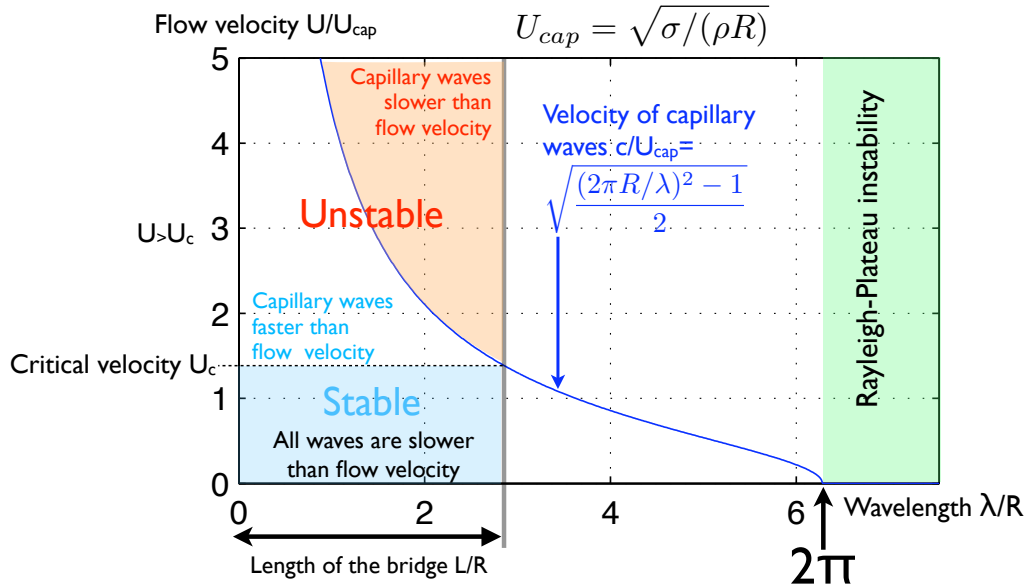
FIGURE 4. A sketch showing how the Rayleigh-Plateau instability is a particular case of the instability of the bridge with throughflow. For simplicity we have used the dispersion relation valid for long waves from §3.1 which we have used in the paper. For the full dispersion relation, see for instance Rayleigh (1879); Chandrasekhar (1981).

capillary Venturi. This is illustrated in figure 4

$$\frac{U_{crit}}{U_{cap}} = \sqrt{\frac{(2\pi R/L)^2 - 1}{2}}. \tag{2.3}$$

3. 1D nonlinear model

To refine this analysis and dwell upon the structure of the nonlinear bifurcations, we now introduce a 1D model of the flow through a cylindrical ligament from Eggers & Dupont (1994). This model assumes wavelength long compared to the radius and retain the full expression of the capillary pressure jump through the tensed interface

$$\begin{aligned}
u_t &= -uu_x - \frac{p_x}{\rho} + \frac{3\nu(r^2 u_x)_x}{r^2} \\
p &= \sigma\left[\frac{1}{r(1+r_x^2)^{1/2}} - \frac{r_{xx}}{(1+r_x^2)^{3/2}}\right] \\
r_t &= -ur_x - \frac{1}{2}u_x r \\
u(0) &= U, r(0) = R, r(L) = R,
\end{aligned} \tag{3.1}$$

with u the longitudinal velocity (in the x direction), r the radius, ν the fluid kinematic viscosity, σ the surface tension and ρ the fluid density. Please see Eggers & Villermaux (2008) for several examples of the use of this model.

3.1. Dispersion relation

We now proceed to derive the dispersion relation for low amplitude harmonic waves on an infinite cylinder of liquid at rest. This dispersion relation will give us the expression of the wavespeed that we will compare to (2.2).

We assume a small perturbation $r = R + \tilde{r}, u = U + \tilde{u}, p = \sigma/R + \tilde{p}$ to the cylindrical

steady state. Since here we do not have upstream and downstream boundary conditions, by galilean invariance, we can assume $U = 0$. Since we are interested in the low viscosity regime, we assume $\nu = 0$. We linearize (3.1) by injecting these expressions. We obtain

$$\tilde{u}_t = -\tilde{p}_x/\rho$$
$$\tilde{p} = -\sigma(\tilde{r}/R^2 + R_{xx})$$
$$\tilde{r}_t = -R\tilde{u}_x/2.$$

We now assume harmonic waves for $\tilde{u}, \tilde{p}, \tilde{r}$, for instance for $\tilde{u}$:

$$\tilde{u} = \hat{u}e^{i\alpha x + st},$$

with α the wavenumber and s the temporal exponential growth rate. We obtain

$$s^2 = \frac{\sigma}{\rho R}\frac{\alpha^2(1 - R^2\alpha^2)}{2}.$$

The growth rate s is purely imaginary (traveling neutral waves) whenever $1 - R^2\alpha^2$ is negative, i.e. when the wavelength $\lambda = 2\pi/\alpha$ is less than the perimeter of the cylinder $2\pi R$. Otherwise waves are unstable: this is the Rayleigh-Plateau instability. We are interested in the wavespeed of neutral waves. The speed is

$$c = -\frac{\text{Imag}(s)}{\alpha} = \sqrt{\frac{\sigma}{\rho R}}\sqrt{\frac{R^2\alpha^2 - 1}{2}}$$

thus we recover the capillary wavespeed of §2.2 (2.2).

3.2. *Bifurcation diagram*

We compute the bifurcation diagram for steady states of the nonlinear 1D model. The code is written in Octave/Matlab language. The unknowns u, r, p are discretized in space using Chebychev pseudospectral differentiation, see Weideman & Reddy (2000). The boundary conditions are imposed in the discretized version of the system by replacing the equations for the first and last gridpoints by the equations of the boundary conditions. The nonlinear steady solutions of the system are computed by iterating the Newton-Raphson method and using the Jacobian calculated analytically from the linearization of (3.1). We found that about 100 gridpoints (Chebychev colocation nodes) in the axial direction provide a satisfactory accuracy of the computations.

For these computations, we use a mean radius $R = 1$, surface tension $\sigma = 1$ and fluid density $\rho = 1$. The Reynolds number is $Re = UR/\nu$, the Ohnesorge number is $Oh = \mu/\sqrt{\rho\sigma R} = \nu$, the Weber number is $We = \rho R U^2/\sigma = U^2$, and the capillary velocity $U_{cap} = \sqrt{\sigma/(\rho R)} = 1$.

To compute the bifurcation diagram, we perform a Keller pseudo-arclength numerical continuation method, see Keller (1982), based on the continuation parameter U. The computation is initialized with $U = 0$ and the initial guess for the Newton-Raphson iterations is the trivial straight bridge solution at $V/V_0 = 1$.

We draw in figure 5 the bifurcation diagram for the perfect cylinder ($V/V_0 = 1$ and inviscid flow $\nu = 0$), and for an imperfect system (volume slightly less than the cylinder $V/V_0 = 0.99$ and viscous $Oh = \nu = 0.01$). To represent the changes in the steady state of the bridge while increasing U, we draw the slope of the free surface at the inlet. For the perfect bridge, we see that the straight cylinder always remains a steady state of the system, and has several successive pitchfork bifurcations. At these bifurcations, the straight solution branches with a nontrivial steady solution shown on the figure. Since the system is stable for low velocity (subcritical bifurcation), we know that the pitchfork

10   *G. Paré and J. Hoeffner*
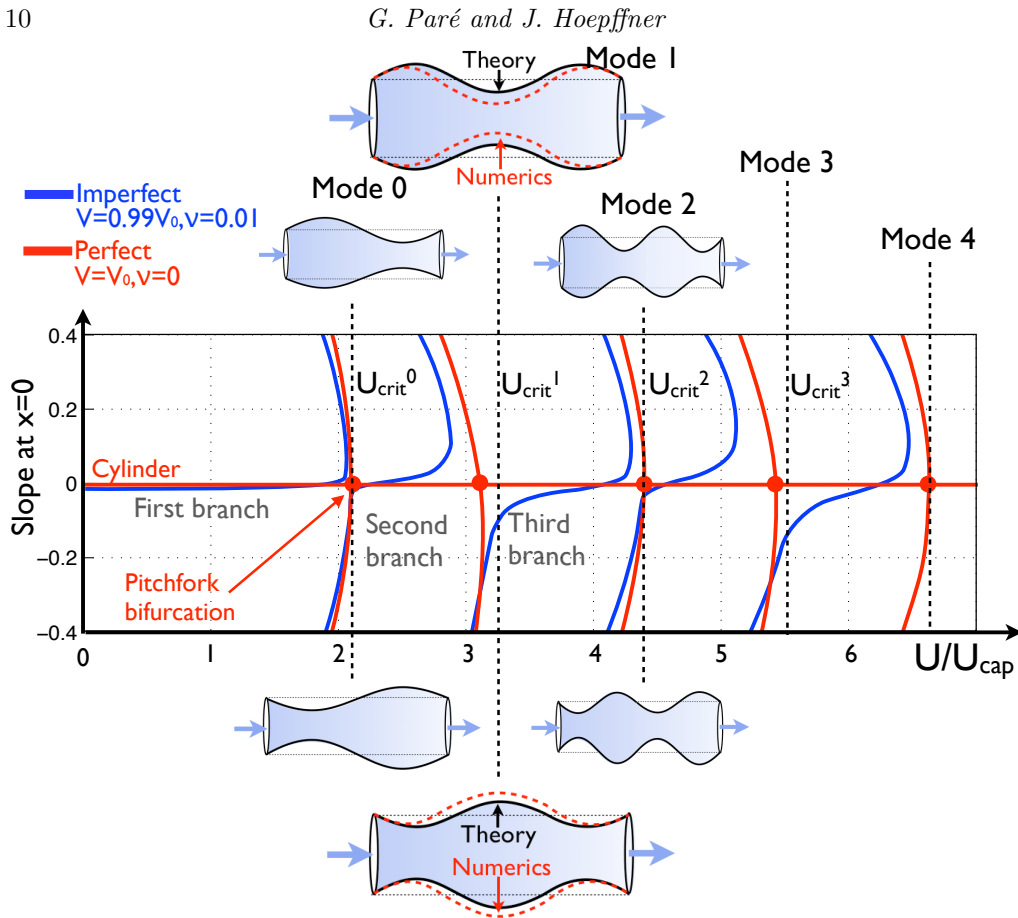
FIGURE 5. Bifurcation diagram of the straight cylinder with throughflow. It is obtained by numerical continuation of (3.1). We show two cases, the *perfect* case with a straight cylinder and inviscid fluid, and an *imperfect* case with a volume slightly less than the straight cylinder and a small viscosity. The vertical dashed lines show the prediction of instability threshold from (2.1). We name *first, second, third* ... the successive branches of nonlinear solutions separated by pitchfork bifurcations.

corresponds to a destabilization of the system. Thus the straight bridge with throughflow becomes unstable after the first bifurcation.

We have drawn as vertical dashed lines the critical velocities predicted in §2.2 by (2.3) for the successive waves allowed by the boundary conditions

$$\frac{U^i_{crit}}{U_{cap}} = \sqrt{\frac{(2\pi R/\lambda_i)^2 - 1)}{2}}.$$

with $\lambda_0 = L$ a sinus that spans the entire bridge (called "mode 0" on the figure), $\lambda_1 = L/1.5$ for which the length of the bridge is spanned by 1.5 wavelengths, and $\lambda_2 = L/2, \lambda_3 = L/2.5, \lambda_4 = L/3$. We see that the first bifurcation is accurately predicted by the theory. This validates that indeed, the velocity at which the system becomes supersonic corresponds to a bifurcation and a loss of stability.

This accuracy is also found for all even modes. As opposed to the band-saw, the capillary bridge is a dispersive system. Here, waves with short wavelengths travel faster than longer waves. As we progressively increase the throughflow, the system becomes

supersonic with respect to each successive modes allowed for by the boundary conditions. Each of these transitions corresponds to a pitchfork in the bifurcation diagram.

We see on the other hand that the location of the pitchfork is slightly overestimated for uneven modes. A mode of surface oscillation is allowed by the boundary conditions if the free surface deformation is zero at $x = 0$ and $x = L$, this selects the wavelengths $2L, L, L/1.5, L/2, \ldots$. On the other hand, the modes should as well satisfy volume conservation, this is why the wavelength $2L$ is forbidden in the system: a free surface deformation cannot be only positive, it should have both ups and downs. For the same reason, uneven modes are not exact solutions of the system, since for instance mode 1 has two ups and only one down. We see nevertheless that there exists a mode with nearly this shape. We have sketched this modification for mode 1 on the figure. This is why the critical velocity predicted by sinusoidal waves is close to the correct bifurcation of uneven modes but not equal.

We have also drawn the bifurcation diagram for a slightly imperfect bridge. This corresponds to a volume slightly less than the cylinder for a fluid with a small viscosity. We see that the pitchforks transform into imperfect bifurcations and the straight bridge solution disappear above the first bifurcation.

4. Simulations of the Navier-Stokes equations

We have described the dynamic instability for a cylindrical capillary Venturi ($V/V_0 = 1$) using a theoretical approach in §2.2 and by computing the bifurcation diagram of a 1D nonlinear model in §3. We proceed now to a third step of modeling, using numerical simulations of the Navier-Stokes equations. We use the open-source software Gerris Flow Solver, as described in Popinet (2009).

The Navier-Stokes equations are discretized using finite volumes and the interface is tracked using the Volume Of Fluid method. We assume an axisymmetric solution. The inflow and outflow pipes are solids of inner radius 1 and thickness 0.05 with a no-slip boundary condition. The tip of each pipe is made smooth in the shape of half a circle. The computational box has height $H = 2$. The liquid has density $\rho = 1$ and kinematic viscosity $\nu = 0.01$ (thus $Oh = 0.01$). The outer gas has density 0.01 and kinematic viscosity 0.0001. We use a quad-tree adaptive mesh with a criterion for refinement based on vorticity and distance from the solid boundaries and free surface. We use seven levels of refinement of the tree structure of the mesh, which means that the smallest mesh element has size $1/2^7 = 0.0078$.

The inflow is a flat velocity profile at a distance $\ell_{in} = 1.5$ upstream of the start of the capillary bridge and the outflow is a flat velocity profile—just as the inflow and with the same flux. The outflow is at distance $\ell_{out} = 1.5$ downstream of the end of the capillary bridge. We have chosen a flat inflow velocity profile because the original motivation of this study was the flow in the neck of a retracting ligament as discussed in the introduction. In the moving reference frame of the neck, the inflow is a plug flow. In our simulations, the breakup happens at Reynolds numbers of the order of 100. The *entrance length* in a pipe is the distance from the flat inflow profile down to the fully developed parabolic profile. This length is commonly estimated at about 0.1 times the Reynolds, times the radius of the pipe. Thus here, 10 radius downstream; well after the capillary bridge. We have validated our numerical results by checking that varying the length of the inflow and outflow pipes has only a small impact on the critical velocity for breakup.

The two triple points where the solid pipe, the liquid and the gas meet are pinned at the tip of the pipes, which means a reference radius $R = 1.025$ for the capillary bridge in the numerical simulations. At the pipe walls, we impose a contact angle of 90 degrees

for the free surface. Only when the bridge breaks up, the strong associated pressures and velocities can induce depinning of the triple point. We do not use a proper model for the motion of the contact line, so the flow near the triple point is not accurately described during the depinning.

The protocol for our simulations is the following:

(a) We start with a cylindrical bridge with no flow

(b) We slowly pump fluid through the inflow and outflow pipes until reaching the desired bridge volume V/V_0.

(c) We then increase progressively the throughflow. This increase should be slow enough as to ensure a quasistatic behaviour, we choose a flux $Q = \pi R^2 t/300$ for all simulations.

(d) We record the evolution with throughflow of the minimum radius of the capillary bridge.

The results are shown in figure 6. We observe in these simulations two different behaviors. For volumes V/V_0 close to one, the bridge keeps an approximately cylindrical shape until a critical velocity where it suddenly builds a neck upstream and starts to show self-sustained nonlinear oscillations. We have drawn the critical velocity predicted from our theory of §2.2, $U_c = 0.86$ with a black circle. We see that the critical velocity is overpredicted, this is because the volume of this bridge is 0.93, less than the cylinder. A better agreement is seen in the following figure 7 where we show volumes closer to 1. The second behaviour happens for lower volumes, where the neck suddenly moves downstream and then quickly breaks up.

These two different behaviors are understood by drawing the nonlinear bifurcation diagram of (3.1) on the figure. Here, instead of showing the slope of the interface at inflow as we did in figure 5, we show the evolution of the minimum radius of the bridge (the neck). This measure is a more robust account of the similarities between the time marching of the Navier-Stokes equations and the 1D model. We show only the two first branches of the bifurcation diagram of the 1D model. We can observe here two interesting things. First, the second branch is in fact a closed loop, and it has a portion unstable to an oscillatory instability (a Hopf bifurcation); this portion corresponds to a bridge with a neck located upstream as sketched in figure 1. When increasing quasistatically the throughflow, the system reaches its first critical velocity (2.1). It then leaves the first branch and jumps to the second branch, with a neck upstream. This branch is Hopf-unstable but we see that there is a saturation mechanism that yields a nonlinear orbit. The mean neck radius of the orbit follows the nonlinear branch when increasing velocity. When we reach the critical velocity for the second branch, the bridge eventually breaks up.

When the volume is low, the second branch is harder to reach when jumping from the first one, or the second branch may even disappear because of viscosity. In this case, the bridge directly breaks up.

In figure 7 we show an overview of the different simulations that we have performed. This data can be read just as for the previous figure 6; we just show more values of the bridge volume V/V_0 and show three values of the bridge aspect ratio $L/R = 3, 4, 5$. We show the theoretical critical velocity with a black circle labelled U_c. We see that, as the volume of the bridge tends to 1, the critical velocity of the breakup indeed tends to the theoretical prediction.

All these simulations are summarized in figure 8. We show how the breakup boundary depends on the throughflow. When U increases, the breakup boundary moves up. This means that with a throughflow, the bridge is no longer able to sustain a low volume. We have distinguished as shaded area the parameter ranges for which there are nonlinear
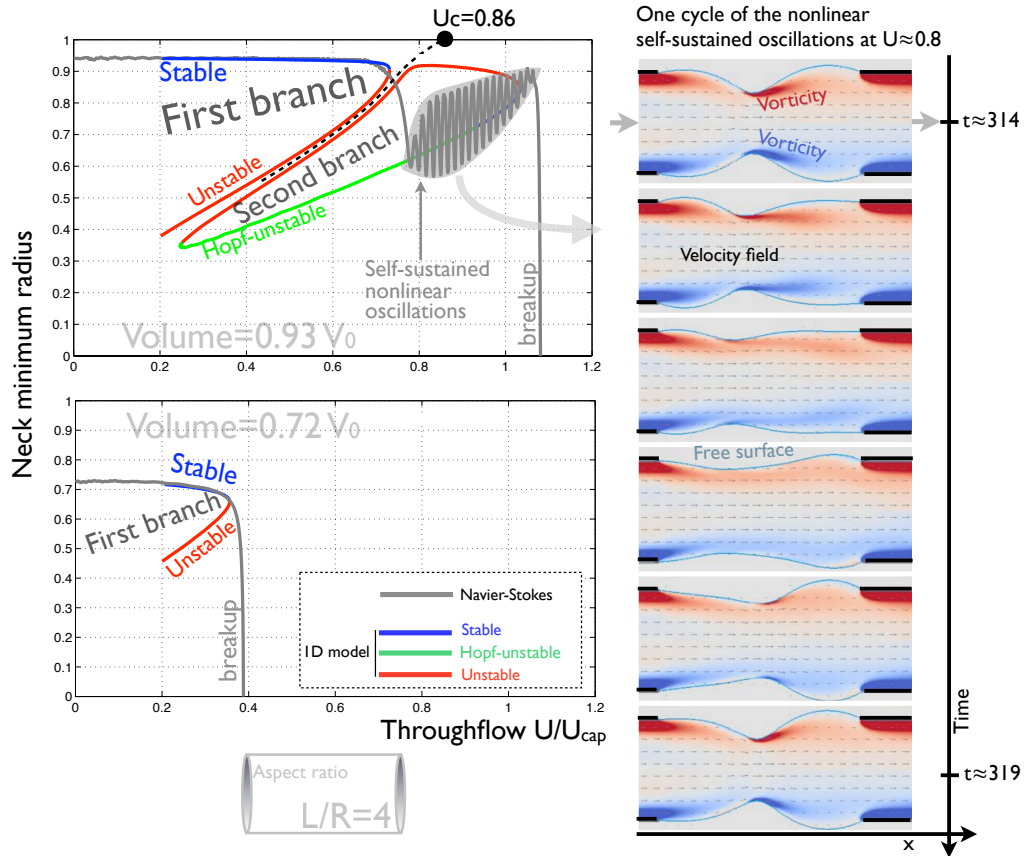
FIGURE 6. Comparison of the bifurcation diagram for the 1D nonlinear model of Eggers & Dupont (1994) and Navier-Stokes simulations. For these simulations, $\nu = Oh = 0.01$. For a volume close to 1, we observe nonlinear self-sustained oscillations corresponding to a saturated Hopf instability, and for a low volume, breakup of the bridge. U_c indicates the critical velocity for the cylindrical case from (2.1).

oscillations. These boundaries are extracted from figure 7 as follows: the left limit of the shaded areas means that the simulation jumps from the first branch to the second branch, and the right limit means that the bridge breaks up. If the bridge breaks up without oscillations, the two limits are the same and there is no shaded area. In these simulations we progressively increase with time the throughflow, slowly enough so that the evolution is quasistatic. We observe on the other hand not such a good fit for the breakup boundary for static bridges. This means that it was not quasistatic enough for this particular case.

5. Discussion

We have discussed in details the behaviour of a capillary bridge with throughflow. We propose this system as an archetypal configuration to understand how a flow can affect the free-surface in which it is contained. Our first result is that the straight bridge will destabilize when the fluid velocity is larger than the phase velocity of the slowest capillary wave. This slowest capillary wave is the longest one, the one that spans the complete length of the bridge.
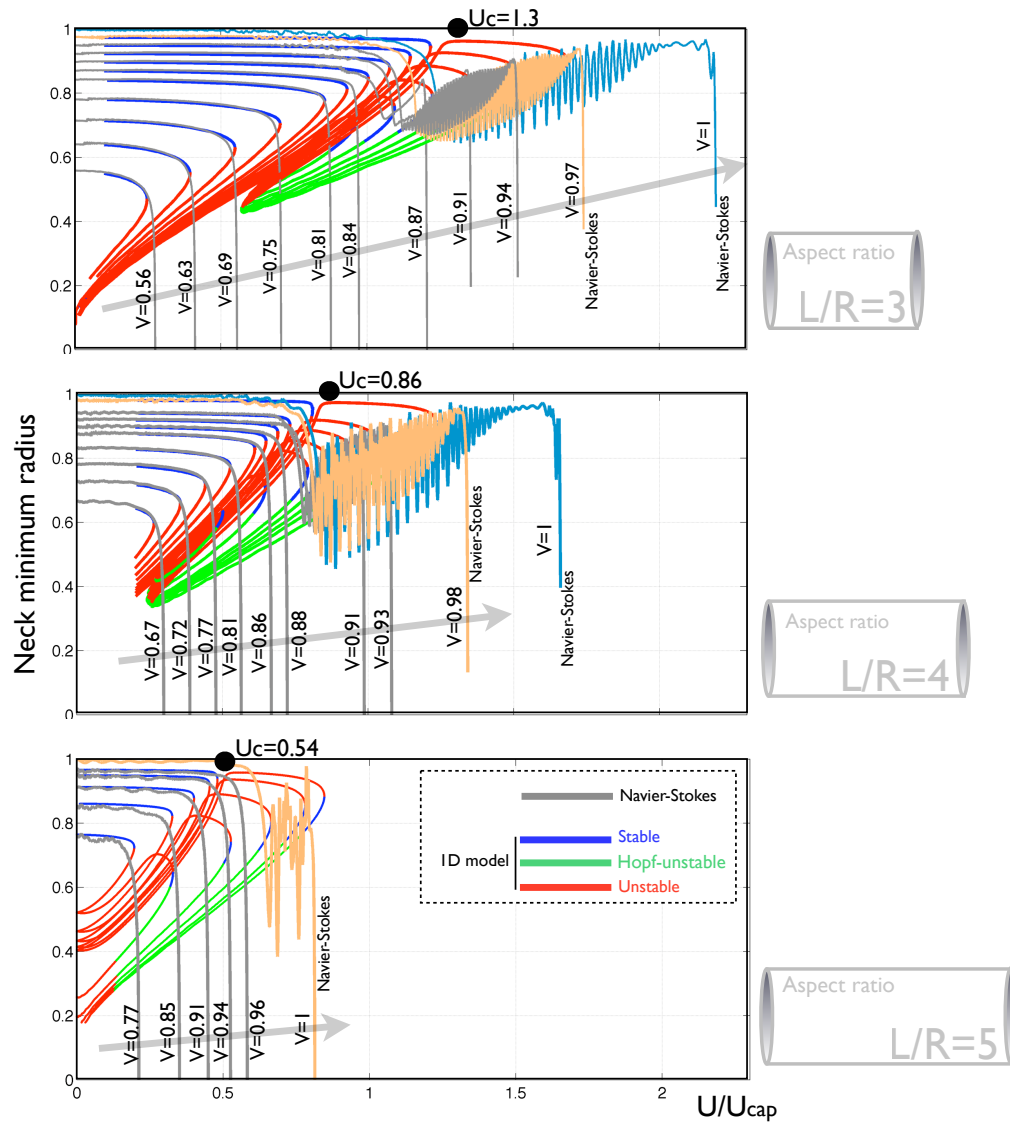
FIGURE 7. Overview of the numerical simulations and bifurcation diagrams of the capillary Venturi. We see the breakup and the self-sustained oscillations. U_c indicates the critical velocity for the cylindrical case from (2.1). For these simulations $\nu = Oh = 0.01$.

We compared the nonlinear bifurcation diagram of a 1D model to numerical simulations of the Navier-Stokes equations. When progressively increasing the throughflow, the numerical simulations follows the first branch which is stable, with the neck radius progressively decreasing. When approaching the velocity of the slowest capillary wave, the first branch has a fold bifurcation. At this point, the Navier-Stokes equations jump to a second branch, unstable because of a Hopf bifurcation. We observe that the instability saturates such that the simulation follows a nonlinear orbit. If we continue to increase the throughflow, the simulation follows the second branch until a second fold bifurcation where the bridge breaks up. If the volume of the bridge is too low, instead of jumping to the second branch, the bridge breaks directly.

The capillary Venturi 15
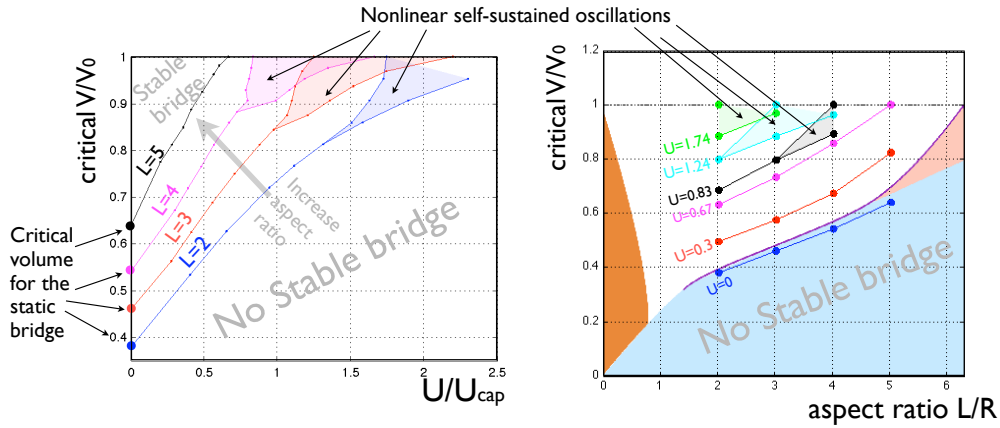
FIGURE 8. Overview of the dynamic behaviour of the simulations of the Navier-Stokes equations.

We have restricted our numerical study to axisymmetric bridges. With the software Gerris, we could have performed full 3D simulations but the computational cost would have been large. We have started to perform laboratory experiments of the capillary Venturi. Our preliminary observation is that the breakup of the bridge happens through an axisymmetric instability. For the experimental parameters leading to nonlinear self-sustained oscillations, the destabilization starts as a axisymmetric shape, but may later turn into a 3D oscillation through a secondary instability. In the experiment, gravity plays a strong role. We were not able to reduce the size of our apparatus in order to render gravity negligible, so we did not include the experimental results here.

In the present paper, we have discussed the stability properties of the capillary bridge but not the possibility of complete detachment of the jet at the neck. This behavior can be expected by analogy with the Venturi flow with solid walls. Some preliminary experiments show that there indeed exist stable steady states that are fully detached. We currently study this in details, and we are particularly interested in the adaptation of the free surface shape to the different configurations of the inner flow. For an experiment in this context, please see Sébilleau *et al.* (2009). In that paper, a jet is impinging from above to the surface of a bath at rest. It is shown that the fluid from the jet can either spread along the flat surface (attached flow) or pierce it (detached flow) depending on inertia, viscosity and surface tension.

We conclude with a discussion of the experiment of breakup of a flat capillary bridge in microgravity of Conrath *et al.* (2013). Their figure 6 is an equivalent to our figure 8, where they report what are the length/velocity of stable bridges. Unfortunately, they did not use the volume of the bridge as a control parameter. As a consequence, they do not have a case equivalent to our $V/V_0 = 1$ for which the criterion of stability in terms of capillary wave velocity is most accurate. Nevertheless, we can demonstrate here a first comparison of our theory for breakup and their experimental data. This is shown in figure 9. We have drawn on their graph the line along which the throughflow is equal to the speed of the slowest capillary wave. Here we consider a capillary wave on a flat surface whose velocity is (see Guyon *et al.* (2001))

$$c = \sqrt{\frac{\sigma}{\rho} \frac{\alpha}{\tanh(\alpha d/2)}},$$

with the wavenumber of the longest (and slowest) wave $\alpha = 2\pi/L$ and d is the distance
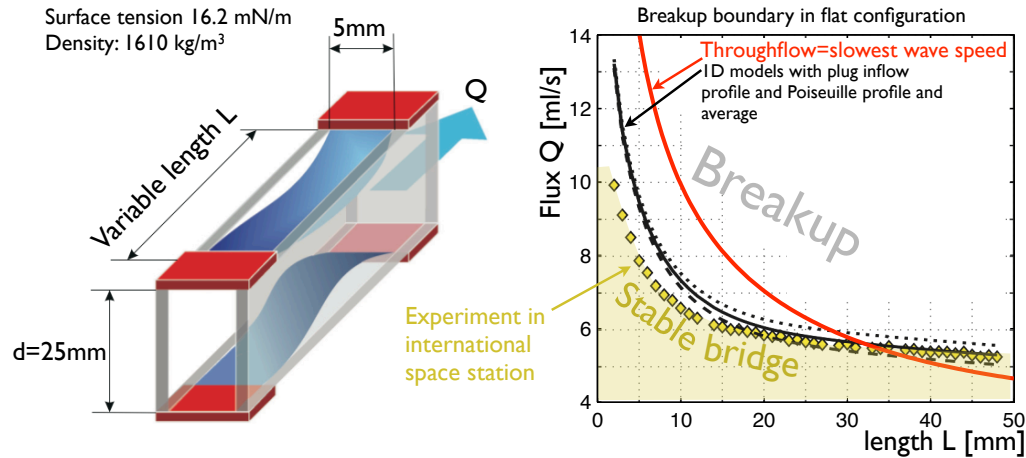
FIGURE 9. Figure adapted from the microgravity experiment of Conrath *et al.* (2013). The line where the throughflow is equal to the slowest capillary wave speed corresponds to our theory.

between the two free surfaces. The tanh accounts for the finite depth of the bridge, on which we assume a varicose deformation. Their figure show the breakup boundary obtained by a 1D model similar to (3.1). For the mean inflow profile in their models, they consider two cases: one with a Poiseuille flow and one with a plug flow.

The comparison is encouraging. For short bridges, the experiment breaks up before the theoretical throughflow, which is compatible with the fact that their V/V_0 is less than one. On the other hand long bridges breakup for supersonic throughflow. This may be explained by two effects. First, the viscous friction between the two flat plates may be stabilizing, and second, the inflow profile is not a plug, but a Poiseuille, which means that the flow velocity at the free surfaces is less than the average that we get from the flux.

To conclude, let us give a few orders of magnitude. According to (2.3), a cylindrical ($V/V_0 = 1$) capillary bridge of water (density $1000Kg/m^3$, surface tension $0.072J/m^2$, dynamic viscosity $\mu = 0.001$) with diameter 2 millimeter and length 4 millimeter (aspect ratio $L/R = 4$) will breakup at velocity $U_{crit} \approx 23cm/s$ which means a critical flux of about 0.7 milliliter per second. To get the other orders of magnitudes for this particular choice of capillary bridge, you just need to multiply the velocities on our graphs by the physical $U_{cap} \approx 27cm/s$.

The critical velocity of this bridge corresponds to a Reynolds number (based on the bridge radius) of about 230. In comparison to this, at critical velocity, the fluid with viscosity $\nu = 0.01$ of our numerical simulation has a Reynolds of about 86 (a bit less than three times more viscous). According to the nonlinear simulations, this bridge will oscillate before breakup with a frequency of roughly $60Hz$. This means approximately one oscillation each throughflow time.

REFERENCES

ATREYA, SRINIVAS & STEEN, PAUL H. 2002 Stability analyses of long liquid bridges in the presence of gravity and flow. *Proceedings: Mathematical, physical and engineering sciences* **458** (2027), 2645–2669.

AVRAAM, D. G. & PAYATAKES, A. C. 1995 Flow regimes and relative permeabilities during steady-state two-phase flow in porous media. *J. Fluid Mech.* **293**.

CHANDRASEKHAR, S. 1981 *Hydrodynamic and hydromagnetic stability*. Dover, New york.

CONRATH, M., CANFIELD, P. J., BRONOWICKI, P. M., MEYER, M. E., WEISLOGEL, M. M. & GRAH, A. 2013 Capillary channel flow experiment aboard the international space station. *Physical review E* **88** (063009).

DAERR, A., EGGERS, J., LIMAT, L/ & VALADE, N. 2011 General mechanism for the meandering instability of rivulets of newtonian fluids. *Phys. Rev. Lett.* **106** (184501).

DATTA, SUJIT S., DUPIN, JEAN-BAPTISTE & WEITZ, DAVID A. 2014 Fluid breakup during simultaneous two-phase flow through a three-dimensional porous medium. *Phys. Fluids* **26** (062004).

DOARÉ, OLIVIER & DE LANGRE, E. 2002 Local and global instability of fluid-conveying pipes on elastic foundations. *Journal of fluid and structures* **16** (1), 1–14.

EGGERS, JENS & DUPONT, TODD F. 1994 Drop formation in a one-dimensional approximation of the Navier-Stokes equation. *J. Fluid Mech.* **262**, 205–221.

EGGERS, JENS & VILLERMAUX, EMMANUEL 2008 Physics of liquid jets. *Rep. Prog. Phys.* **71** (036601).

EVERETT, D. H. & HAYNES, J. M. 1972 Model studies of capillary condensation 1. cylindrical pore model with zero contact angle. *J. Colloid Interface Sci.* **38** (1), 125–137.

GALLAIRE, FRANCOIS, RUITH, MICHAEL, MEIBURG, ECKART, CHOMAZ, JEAN-MARC & HUERRE, PATRICK 2006 Spiral vortex breakdown as a global mode. *J. Fluid Mech.* **549**, 71–80.

GRAND-PITEIRA, NOLWENN LE, DAERR, ADRIAN & LIMAT, LAURENT 2006 Meandering rivulets on a plane: A simple balance between inertia and capillarity. *Phys. Rev. Lett.* **96** (254503).

GUYON, ETIENNE, HULIN, JEAN-PIERRE, PETIT, LUC & MITESCU, CATALIN D. 2001 *Physical Hydrodynamics*. Oxford University Press, Oxford.

HEIL, MATTHIAS & HAZEL, ANDREW L. 2011 Fluid-structure interaction in internal physiological flows. *Annu. Rev. Fluid Mech.* **43**, 141–162.

HEIL, MATTHIAS & JENSEN, OLIVER E. 2003 *Flows in deformable tubes and channels*, chap. 2. John Wiley and Sons Limited.

HOEPFFNER, JÉRÔME & PARÉ, GOUNSÉTI 2013 Recoil of a liquid filament: escape from pinch-off through creation of a vortex ring. *J. Fluid Mech.* **734**, 183–197.

HUERRE, P. & MONKEVITZ, P. A. 1990 Local and global instabilities in spatially developing flows. *Annu. Rev. Fluid Mech.* **22**, 473–537.

JOSEPH, D.D., BAI, R., CHEN, K.P. & RENARDY, Y.Y. 1997 Core-annular flows. *Annu. Rev. Fluid Mech.* **29** (1), 65–90.

KELLER, HERBERT B. 1982 Continuation methods in computational fluid dynamics. In *Numerical and physical aspects of aerodynamic flows* (ed. Tuncer Cebeci), pp. 3–14. Springer New York.

KELLER, JOSEPH B. 1983 Breaking of liquid films and threads. *Phys. Fluids* **26**, 3451–3453.

KIRSTETTER, GEOFFROY, RAUFASTE, CHRISTOPHE & CELESTINI, FRANK 2012 Jet impact on a soap film. *Physical review E* **86** (036303).

LOWRY, BRIAN JAMES & STEEN, PAUL H. 1995 Capillary surfaces: stability from families of equilibria with application to the liquid bridge. *Proceedings: Mathematical and physical sciences* **449** (1937), 411–439.

MOTE, C. D. 1965 A study of band saw vibrations. *Journal of the Franklin institute* **279** (6), 430–444.

PLATEAU, JOSEPH 1873 *Statique expérimentale et théorique des liquides soumis aux seules forces moléculaires*. Gauthier-Villars, Paris.

POPINET, STÉPHANE 2009 An accurate adaptive solver for surface-tension-driven interfacial flows. *J. Comp. Phys.* **228**, 5838–5866.

RAYLEIGH 1879 On the instability of jets. *Proc. Lond. Math. Soc.* **10**, 4–13.

RICHARDS, L. A. 1931 Capillary conduction of liquids through porous mediums. *Physics* **1** (1), 318–333.

ROSENDAHL, UWE, OHLHOFF, ANTJE & DERYER, MICHAEL E. 2004 Choked flows in open capillary channels: theory, experiments and computations. *J. Fluid Mech.* **518**, 187–214.

RUSSO, MATHEW J. & STEEN, PAUL H. 1989 Shear stabilization of the capillary breakup of a cylindrical interface. *Phys. Fluids* **1** (12).

SÉBILLEAU, J., LIMAT, L. & EGGERS, J. 2009 Flow separation from a stationary meniscus. *J. Fluid Mech.* **633**, 137–145.

18 *G. Paré and J. Hoepffner*

Slobozhanin, Lev A. & Perales, José 1993 Stability of liquid bridges between equal disks in an axial gravity field. *Phys. Fluids* **5** (6).

Stone, Howard A. & Leal, L. G. 1989 Relaxation and breakup of an initially extended drop in an otherwise quiescent fluid. *J. Fluid Mech.* **198**, 399–427.

Thomson, William 1871 Hydrokinetic solutions and observations. *Phil. Mag. series 4* **42**, 362–377.

Ulsoy, A. G., Mote, C. D. & Szymani, R. 1978 Principal developments in band saw vibration and stability research. *Holz als Roh- und Werkstoff* **36**, 273–280.

Weideman, J. A. C. & Reddy, S. C. 2000 A Matlab differentiation matrix suite. *ACM Transactions on Mathematical Software* **26** (4), 465–519.